# Wavelet analysis of chaotic time series

J.S. Murguía and E. Campos-Cantón
*Departamento de Físico Matemáticas, Universidad Autónoma de San Luis Potosí, Alvaro Obregón 64, 78000 San Luis Potosí, S.L.P., México.*

Recibido el 14 de noviembre de 2005; aceptado el 8 de diciembre de 2005

In this work we analyzed experimental chaotic time series data from three known chaotic systems using the orthogonal wavelet transform. The experimental electronic implementation of the chaotic systems was used to analyze them. The wavelet analysis of the experimental chaotic time series, with a simple statistical approach, gives us useful information of such systems through the energy concentration at specific wavelet levels.

*Keywords:* Chaotic time series; wavelets.

En este trabajo analizamos información de series de tiempo caóticas experimentales de tres sistemas caóticos conocidos, usando la transformada ortogonal ondeleta. Se llevó a cabo la implementación experimental electrónica de los sistemas caóticos, para su respectivo análisis. El análisis ondeleta de las series de tiempo caóticas experimentales, con un simple enfoque estadístico, nos da información útil de dichos sistemas, mediante la concentración de energía en ciertos niveles ondeleta.

*Descriptores:* Series de tiempo caóticas; ondeletas.

PACS: 05.45.-a; 05.45.Tp

## 1. Introduction

Chaotic behavior occurs in many experimental physical phenomena. Various nonlinear electronic systems with this behavior have been constructed [4, 6, 7]. Making measurements on such electronic chaotic circuits result in data with different characteristics. Generally, these experimental data are presented as a *chaotic time series*(CTS). This CTS provides useful information for analysis and interpretation of the physical system that produced it. It is interesting to determine some of the system's key properties by quantifying certain features of the CTS. These properties can then help us to understand the system's behavior in the future.

Different methods arising from scientific investigation have been introduced to analyze these CTS. Fourier analysis is a well established and suitable tool for analyzing stationary time series, whose statistical properties do not vary with time. The Fourier technique decomposes a signal into harmonic components, where the basis functions are trigonometric functions. Another tool for analyzing time series is the wavelet transform(WT) [10, 11]. The WT has been introduced and developed to study a large class of phenomena such as image processing, data compression, chaos, fractals, etc. The basic functions of the WT have the key property of localization in time(or space) and in frequency, contrary to what happens with trigonometric functions. In fact, the WT works as a mathematical microscope on a specific part of a signal to extract local structures and singularities [10, 11]. This makes the wavelets ideal for handling non-stationary and transient signals, as well as fractal-type structures. Because WT is a useful tool, many general aspects of nonlinear time series analysis are reviewed in Refs. 1 and 9.

The goal of the current paper is to analyze experimental CTS using the logarithmic variance of the orthogonal wavelet coefficients [2, 3]. The experimental CTS that we analyzed are from three electronic systems called the Chua, Rössler, and a chaotic generator circuit. These systems exhibit chaotic dynamics. Their dynamics are extremely nonlinear, highly sensitive, and display short time correlations and a broad range of frequencies. In these cases, the Fourier transform(FT) does not appropriately describe the chaotic dynamics. On the other hand, the WT seems as a natural tool for describing them [2, 3].

The structure of this paper is as follows. Section 2 presents an overview of the wavelet transform in the continuous and discrete versions. The experimental setup of the three electronic chaotic circuits is briefly discussed in Sec. 3. Section 4 gives the analysis applied to the experimental chaotic time series. Finally, conclusions are presented in Sec. 5.

## 2. The Wavelet Transform

Let $L^2(\mathbb{R})$ denote the space of all square integrable functions in $\mathbb{R}$. In signal processing parlance, it is the space of functions with finite energy. Let $\psi(t) \in L^2(\mathbb{R})$ be a fixed function. The function $\psi(t)$ is said to be a *wavelet* if and only if its FT $\hat{\psi}(\omega)$ satisfies

$$C_\psi = \int_0^\infty \frac{|\hat{\psi}(\omega)|^2}{|\omega|} d\omega < \infty. \tag{1}$$

The relation (1) is called the *admissibility condition* [10–13], which implies that the wavelet must have a zero average

$$\int_{-\infty}^{\infty} \psi(t) dt = \hat{\psi}(0) = 0, \tag{2}$$

and therefore must be oscillatory. In other words, $\psi$ must be a sort of *wave* [10, 11].

Let us define the function $\psi_{a,b}$ by

$$\psi_{a,b}(t) = \frac{1}{\sqrt{a}}\psi\left(\frac{t-b}{a}\right), \tag{3}$$

where $b\in\mathbb{R}$ is a translation parameter, whereas $a\in\mathbb{R}^+$ $(a \neq 0)$ is a dilation or scale parameter. The factor $a^{-1/2}$ is a normalization constant such that $\psi_{a,b}$ has the same energy for all scales $a$. One notices that the scale parameter $a$ in (3) rules the dilations of the spatial variable $(t-b)$. In the same way, factor $a^{-1/2}$ rules the dilation in the values taken by $\psi$.

With (3), one is able to decompose a square integrable function $f(t)$ in terms of dilated–translated wavelets.

We define the *continuous wavelet transform* (CWT for short) of $f(t) \in L^2(\mathbb{R})$ by

$$T_\psi[f](a,b) = \langle f, \psi_{a,b}\rangle = \int_{-\infty}^{\infty} f(t)\bar{\psi}_{a,b}(t)dt$$

$$= \frac{1}{\sqrt{a}}\int_{-\infty}^{\infty} f(t)\bar{\psi}\left(\frac{t-b}{a}\right)dt, \tag{4}$$

where $\langle\ ,\ \rangle$ is the scalar product in $L^2(\mathbb{R})$ defined as

$$\langle f, g\rangle := \int f(t)\bar{g}(t)dt,$$

and the symbol " $^-$ " denotes complex conjugation. The CWT (4) measures the variation of $f$ in a neighborhood of point $b$, whose size is proportional to $a$.

If we are interested in reconstructing $f$ from its wavelet transform (4), we follow the reconstruction formula, also called *resolution of the identity* [10, 11]

$$f(t) = \frac{1}{C_\psi}\int_0^{\infty}\int_{-\infty}^{\infty} T_\psi[f](a,b)\psi_{a,b}(t)\frac{dadb}{a^2}, \tag{5}$$

it is now clear why we imposed (1).

However, some data are represented by a finite number of values, so it is important to consider a discrete version of the CWT (4). Generally, the orthogonal (discrete) wavelet is employed. This method associates the wavelets with orthonormal bases of $L^2(\mathbb{R})$. In this case, the wavelet transform is performed only on a discrete grid of the parameters of dilation and translation, *i.e.* $a$ and $b$ take on only integral values, as will be seen below.

The expansion of an arbitrary signal $x(t)$ on an orthonormal wavelet basis takes the form

$$x(t) = \sum_m\sum_n x_n^m\psi_{m,n}(t), \tag{6}$$

$$x_n^m = \int_{-\infty}^{\infty} x(t)\psi_{m,n}(t)dt, \tag{7}$$

where the orthonormal wavelet basis functions are related according to

$$\psi_{m,n}(t) = 2^{m/2}\psi(2^m t - n), \tag{8}$$

with $m$ and $n$ as the dilation and translation indices, respectively. The family of (8) can be obtained from (3), setting the parameters $a = 2^{-m}$ and $b = n/2^m$.

The contribution of the signal at a particular wavelet level $m$ is given by

$$x_m(t) = \sum_n x_n^m\psi_{m,n}(t). \tag{9}$$

Equation (9) gives us information of the time behavior of the signal within different scale bands, and gives their contribution to the total signal energy. For us, we refer higher levels to higher scales, as is discussed in Ref. 3.

Mallat [11] provides a computationally efficient algorithm for computing efficiently (6) and (7). This algorithm connects, in an elegant way, wavelets and filter banks. Associated with the wavelet function $\psi(t)$ is a corresponding scaling function, $\varphi(t)$, and scaling coefficients, $a_n^m$ [10–13]. The scaling and wavelet coefficients at scale $m$ can be computed from the scaling coefficients at the next finer scale $m+1$ using

$$a_n^m = \sum_l h[l-2n]a_l^{m+1}, \tag{10}$$

$$x_n^m = \sum_l g[l-2n]a_l^{m+1}, \tag{11}$$

where $h[n]$ and $g[n]$ are typically called lowpass and highpass filters in the associated analysis filter bank. Equations (10) and (11) represent the fast wavelet transform (FWT) for computing (7). Conversely, a reconstruction of the original scaling coefficients $a_n^{m+1}$ can be made from

$$a_n^{m+1} = \sum_l \left(h[2l-n]a_l^m + g[2l-n]x_l^m\right), \tag{12}$$

a combination of the scaling and wavelet coefficients on a coarse scale. Equation (12) represents the inverse of FWT for computing (6). It corresponds to the synthesis filter bank.

As discussed in Ref. 2, some degree of regularity is useful on the wavelet basis for the representation to be well behaved. To achieve this, a wavelet function should have $n$ vanishing moments. A wavelet is said to have $n$ vanishing moments, which will be denoted as $\psi_n(x)$, if and only if it satisfies

$$\int_{-\infty}^{\infty} x^k\psi_n(x)dx = 0, \tag{13}$$

for $k = 0, 1, \ldots, n-1$, and

$$\int_{-\infty}^{\infty} x^k\psi_n(x)dx \neq 0, \quad \text{for} \quad k = n.$$

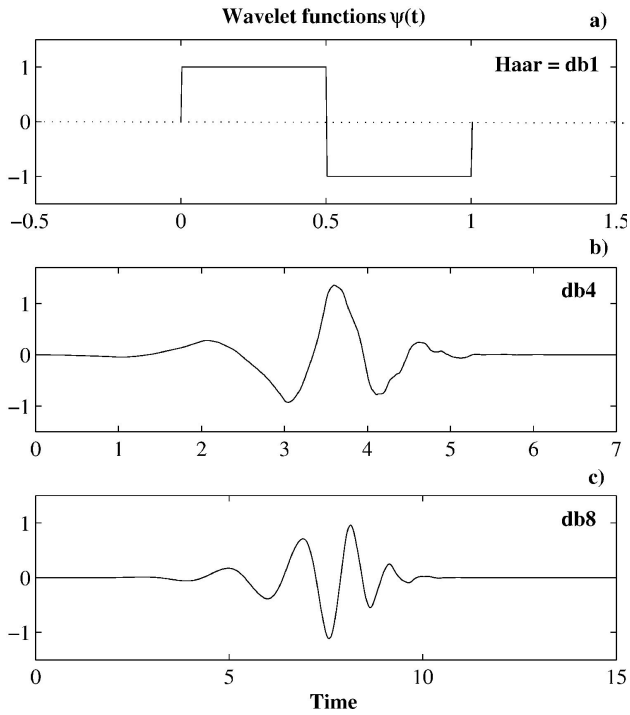


FIGURE 1. Examples of some wavelet functions: (a) Haar wavelet, and Daubechies wavelets b) $db4$, and c) $db8$.

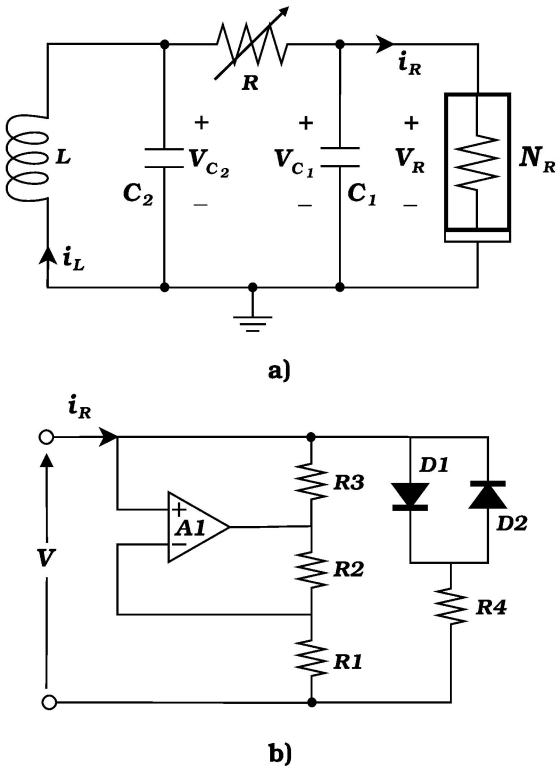


FIGURE 2. Schematic diagrams of a) the Chua circuit, and b) the nonlinear negative resistance $N_R$. The electronic component values, to produce the double scroll attractor, are $C_1$=0.001$\mu$F, $C_2$=0.01$\mu$F, $L$=1.8mH, $R$=5 k$\Omega$, $R1$=750$\Omega$, $R2 = R3 = 220\Omega$, and $R4 = 1.2$ k$\Omega$. The diodes D1 and D2 are 1N914, the operational amplifier A1 is a TL082.

This means that a wavelet with $n$ vanishing moments is orthogonal to polynomials up to order $n-1$. In fact, the admissibility condition (1) requires at least one vanishing moment. So the wavelet transform of $f(x)$ with a wavelet $\psi_n(x)$ with $n$ vanishing moments is nothing but a "smoothed version" of the $n$th derivative of $f(x)$ on various scales. In fact, when someone is interested in measuring the local regularity of a signal this concept is crucial [10, 11].

Figure 1 shows the analyzing wavelet functions that we used in this paper. The Haar wavelet function, shown in Fig 1a, is the simplest wavelet with a closed form. The Daubechies wavelets are determined recursively from its scaling function. Commonly, these wavelets, which are compactly supported, are called DaubN and written as $dbN$, where $N$ corresponds to the order of the function. Some authors use $2N$ instead of $N$. A more detailed treatment of this subject can be found in [10, 11].

## 3. Experimental Setup

In this section, we briefly describe the experimental implementation of three chaotic oscillators, in order to study the experimental chaotic time series. These attractors, despite their simplicity, exhibit chaotic dynamics that have received wide coverage in different areas of mathematics, physics, engineering and others [4, 6–9].

### 3.1. Chua's system

Chua's oscillator is perhaps the simplest circuit that exhibits complex dynamics of bifurcation and chaos. In particular, we are interested in the chaotic attractor called a double scroll oscillator. Chua's circuit, shown in Fig. 2a, consists of two capacitors, one inductor, one potentiometer, and a nonlinear negative resistor (see Fig. 2b).

The dynamics of the Chua's system are modelled by the set of differential equations:

$$\begin{aligned} \dot{x} &= \alpha\,(y - x - f(x))\,, \\ \dot{y} &= x - y + z, \\ \dot{z} &= -\beta y, \end{aligned} \tag{14}$$

where $x(t) = V_{C_1}/V_B$ and $y(t) = V_{C_2}/V_B$ are the voltages across the capacitors $C_1$ and $C_2$, respectively, whereas the current through the inductor $L$ is $z(t) = Ri_L(t)/V_B$. The unit time has been normalized with respect to $(RC_2)^{-1}$. The exact value of the break points of diodes, $V_B$, depends on the nature of diodes (Ge or Si). The parameters $\alpha = C_2/C_1$ and $\beta = R^2C_2/L$. The nonlinear negative resistor has the following $I-V$ characteristic:

$$f(x) = bx + \frac{1}{2}(a-b)\,[\,|x+1| - |x-1|\,]\,, \tag{15}$$

where

$$a = -RR_2/R_1R_3$$

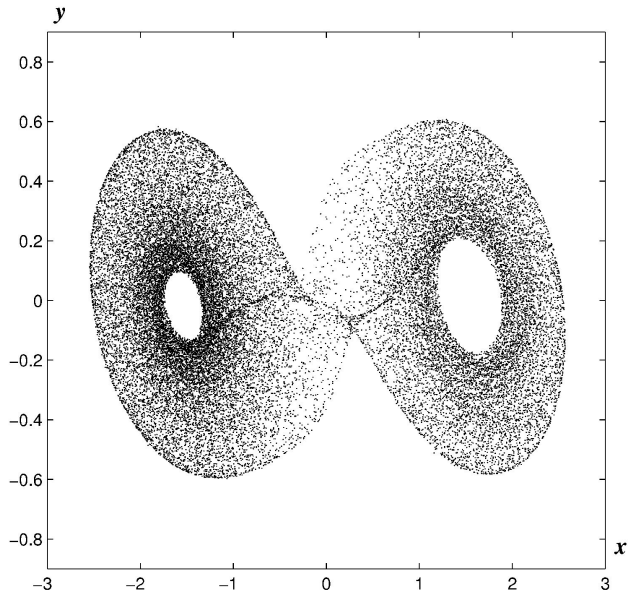


FIGURE 3. Chua's attractor projected on the plane $(x, y)$.

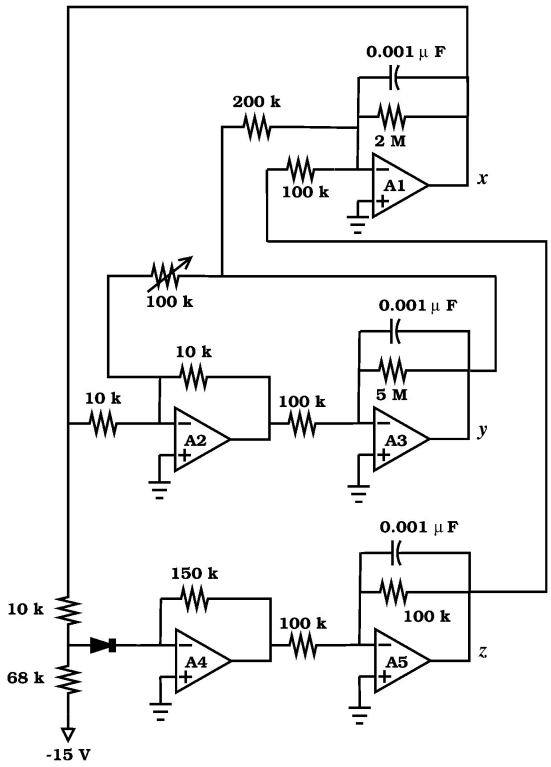


FIGURE 4. The schematic diagram of the chaotic Rössler circuit. All op amps are type TL082, and the diode is 1N914.

and

$$b = -R[(R_2R_4 - R_1R_3)/R_1R_3R_4].$$

A more detailed analysis of the $I - V$ characteristic can be found in Ref. 8. Figure 3 shows the double scroll attractor generated by the Chua circuit of Fig. 2a.

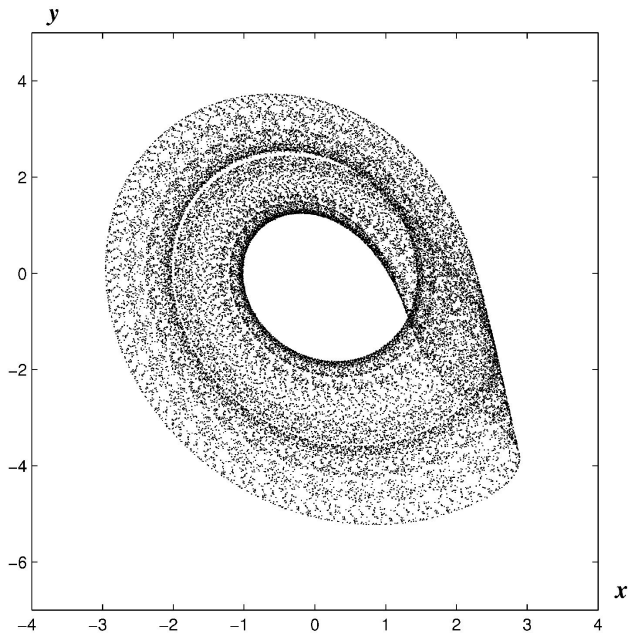


FIGURE 5. Rössler attractor: (a) in $\mathbb{R}^3$, (b)projected on the plane $(x, y)$.

### 3.2. Rössler system

The Rössler experimental circuit that we built in the lab was based on the circuit proposed by Carroll in Fig. 4. The diagram of this circuit is shown in Fig. 4.

The circuit is described by the equations

$$\begin{aligned} \dot{x} &= \alpha(-\Gamma x - \beta y - \lambda z), \\ \dot{y} &= \alpha\left(x + y(\gamma - 0.02)\right), \\ \dot{z} &= \alpha[g(x) - z], \end{aligned} \tag{16}$$

where $\alpha = 10^4$ s$^{-1}$, $\Gamma$ is 0.05, $\beta$ is 0.5, $\lambda$ is 0.133, $\mu$ is 15, and the function $g(x)$ is defined as

$$g(x) = \begin{cases} 0 & \text{if } x \leq 3, \\ \mu(x-3) & \text{if } x > 3. \end{cases}$$

Figure 5 shows the Rössler attractor generated by the schematic diagram of Fig. 4.

### 3.3. Chaotic generator(CG)

This chaotic system has been employed for generalized synchronization between two systems with different parameters [7].

The electronic circuit of the CG is easily implemented in an experimental way, and is shown in Fig. 6a. Depending on the parameter $k$, the behavior of CG can be in regimes of periodic or chaotic oscillations [5, 7], *i.e.* $k$ is the bifurcation parameter.

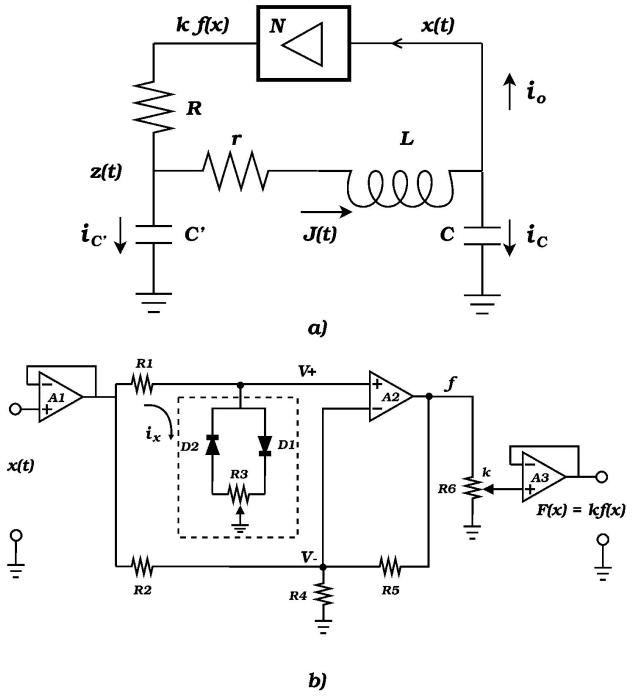


FIGURE 6. Schematic diagrams of a) the chaotic oscillator circuit, and b) of the nonlinear converter N. The component values employed are $C' = 200$ nF, $C = 99.8$ nF, $L = 26.1$ mH, $r = 70\ \Omega$, $R = 1139\ \Omega$, $R1 = 2.7$ k$\Omega$, $R2 = R4 = 7.5$ k$\Omega$, $R3 = 50\ \Omega$, $R5 = 177$ k$\Omega$, and $R6 = 2$ k$\Omega$. The diodes D1 and D2 are 1N4148, the operational amplifiers A1 and A2 are both TL082, and the operational amplifier A3 is LF356N.

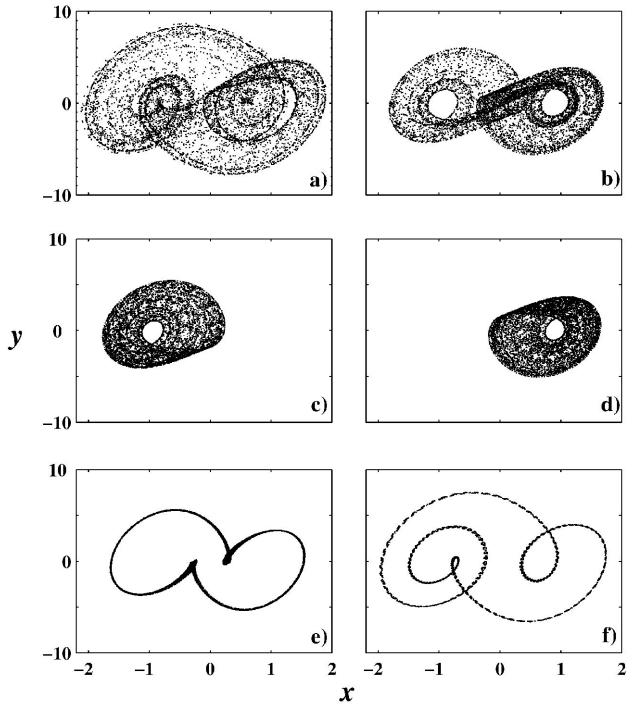


FIGURE 7. The chaotic attractors of the CG projected on the plane $(x, y)$ obtained experimentally for different values of the gain parameter $k$: a) $0.525$, b) $0.465$, c) and d) $0.3865$, e) $0.505$ and f) $0.4605$. Figures c)-d) have different initial conditions.

The dynamics of the CG are modelled by the following set of differential equations:

$$\begin{aligned} \dot{x} &= y, \\ \dot{y} &= z - x - \delta y, \\ \dot{z} &= \gamma\left[kf(x) - z\right] - \sigma y, \end{aligned} \tag{17}$$

where $x(t)$ and $z(t)$ are the voltages across the capacitors $C$ and $C'$, respectively. The parameter $k$ is the gain of the nonlinear converter $N$ at $x = 0$, and $y(t) = J(t)(L/C)^{1/2}$ is the current through the inductor. The unit time has been normalized with respect to $1/\sqrt{LC}$. The parameters $\gamma$, $\delta$ and $\sigma$ depend on physical values of the circuit elements. The nonlinear converter circuit is shown in Fig. 6b. This converter transforms the input voltage $x(t)$ into the output voltage which is expressed by the nonlinear function $F(x) = kf(x)$. The non-linear behavior of the chaotic circuit is due to the functioning of the on-off switch of the pair of diodes. The nonlinear function $f(x)$ is given as

$$f(x) = \begin{cases} \dfrac{[(1-b)(1-w)R_3 - bR_1]x + R_1V_D}{(R_1 + (1-w)R_3)a} & \text{if } x > V_D, \\ \left(\dfrac{1-b}{a}\right)x & \text{if } |x| \le V_D, \\ \dfrac{[(1-b)wR_3 - bR_1]x - R_1V_D}{(R_1 + wR_3)a} & \text{if } x < -V_D, \end{cases} \tag{18}$$

where $w$ is the balance parameter of the variable resistor $R_3$,

$$a = \frac{R_2||R_4}{R_5 + R_2||R_4},$$

$$b = \frac{R_5||R_4}{R_2 + R_5||R_4},$$

and $V_D$ is the break point of the diodes. The function $f(x)$, in (18), considers a sudden commutation of the diodes [5]. A smooth commutation is also discussed in Ref. 5.

The different attractors projected on the plane $(x, y)$, generated by the CG, are shown in Fig. 7. These attractors can be obtained just by changing the gain parameter $k$. We choose the value of the gain $k$ to be equal to $0.525$ and $0.465$ for the attractors of Fig. 7a-b, respectively. These attractors take the shape of a family of double scroll oscillations. For the attractors of Fig. 7c-d, we select the value of $k = 0.3865$, but with different initial conditions. These attractors take the shape of a family of Rössler systems. Whereas in Fig. 7e-f the CG generates thin attractors, which correspond to the values of $k = 0.505$, and $k = 0.4605$, respectively.

## 4. Chaotic Time Series

In order to study experimental CTS, we consider the log variance of the wavelet coefficients as a function of level $m$. In Ref. 3 numerical time series, considered as noise, coherent structure, and chaos were studied. They showed that the variance plot of these time series has a well defined form. If the

variance plot shows a maximum in a particular scale, which means an energy concentration, it often corresponds to a coherent structure. The gradient for a noise time series turned out to be zero in the variance plot; therefore it does not show any energy concentration at specific wavelet level. This statistical approach shows both situations. In certain cases, the gradient of some CTS have a similar appearance with Gaussian noise at lower scales, so that these CTS do not present a fundamental "carrier" frequency at any scale.

The acquired CTS's consist of 32768 data, from the $x(t)$ state, with a sampling rate of 40,000 samples per second for the Rössler and CG systems, and 125,000 samples per second for Chua's system. In this paper, we consider just clean CTS, without noise. However, the possibility of analyzing CTS with noise will be examined in another publication.

The first experimental system examined was Chua's chaotic oscillator. Figure 8a shows a small part of Chua's data, 0.01 seconds. This corresponds to 1,250 points of this CTS. Figure 8b shows a semi-logarithmic plot of the wavelet coefficient variances as a function of level $m$. The $db4$ wavelet was used to obtain this result. At level $m = 11$ there appears a peak, and it is plotted in isolation in Fig. 8c. Despite the fact that a "small" peak appears, there is no indication of a representative energy concentration of the signal at this level. The gradient is close to zero, so that this signal would seem to have noise behavior. On the other hand, Fig. 9 shows a substantial component of the signal. This is the sum of six levels with the major energy concentration. It is useful to see how the shape of the analyzing wavelet is important. Note that there exists a greater similarity with the Haar wavelet (Fig. 9b) with the CTS than the $db4$ wavelet(Fig. 9a). This is because the CTS presents discontinuities, as does the Haar wavelet.

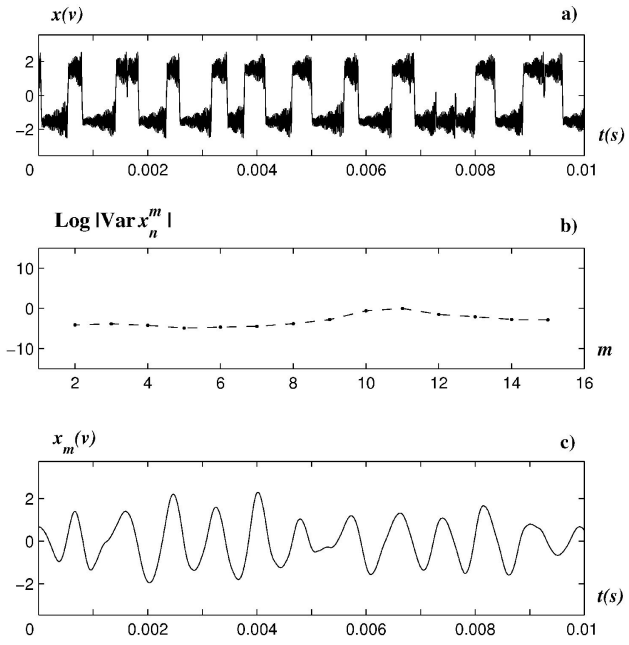


FIGURE 8. a) Experimental time data for Chua's system, b) wavelet coefficient variance, and c) 11th wavelet level.

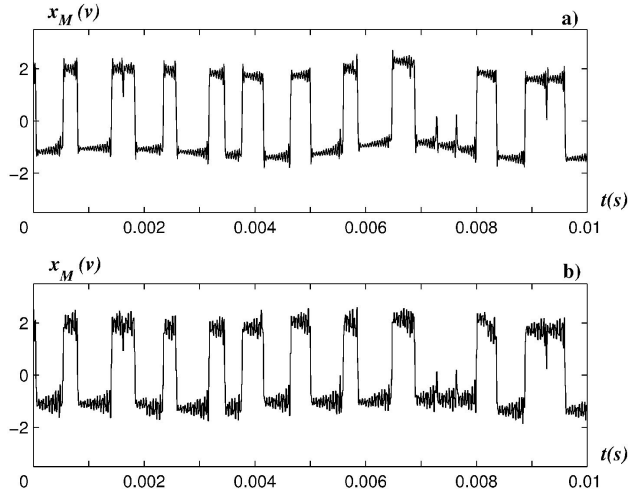


FIGURE 9. Sum of six different wavelet levels with a) $db4$ wavelet, and b) Haar wavelet.

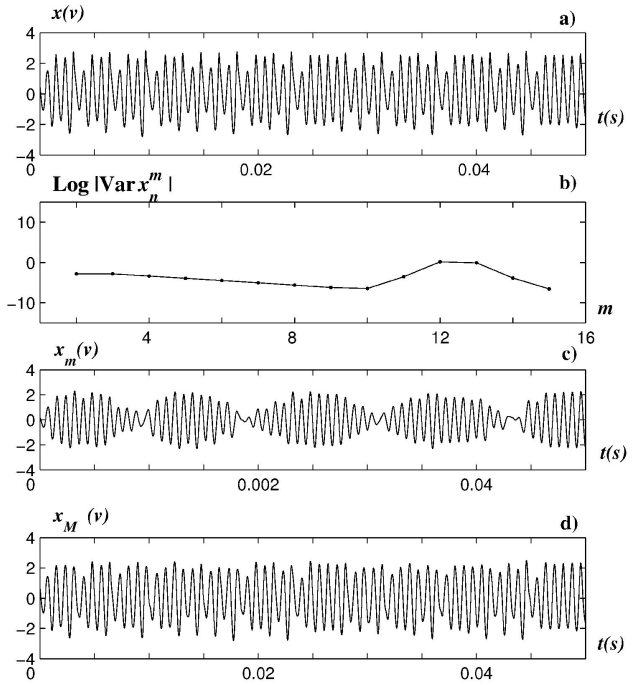


FIGURE 10. a) Experimental time data for Rössler system, b) wavelet coefficient variance, c) 12th wavelet level, and d) sum of 12-13th's wavelet levels.

The second CTS was generated from the Rössler system. Figure 10a shows 0.0512 seconds of Rössler data, which corresponds to 2048 points in the series. The variance plot of the wavelet coefficients is shown in Fig. 10b. The $db8$ wavelet was used to analyze this CTS. The 12th level has the major energy concentration, but it does not properly show the structure of the CTS (see Fig. 10c). We can observe that the whole CTS is dominated by two levels, $m = 12$ and $m = 13$, where the higher energy concentration is found. Therefore, we consider it pertinent to add these levels. In Fig. 10d, we can observe that the most substantial component of the CTS is found at these two levels. In contrast to this experimental re-

sult, [3] presented a numerical time series, and a high energy concentration was found at just one level. However, the high energy concentration at a few levels is a little surprising, both experimentally and numerically. We expected an energy concentration similar to Chua's system since chaotic signals are similar to noise with broadband.

The last CTS's to be analyzed were generated by the CG system. In this case, we consider the CTS's corresponding to attractors of Figs. 7b, d and f. In order to analyze these CTS, the $db8$ wavelet was used.

First of all, we analyze the CTS from the attractor of Fig. 7b. In Fig. 11a shows 0.03 seconds of CG data, 1200 points of the series. The log variance plot of the wavelet coefficient is shown in Fig. 11b, and presents a peak at level $m = 14$. For this case, we can see in Fig. 11c, that there is no representative energy concentration of this CTS. In order to have a substantial component of this CTS, it was necessary to sum six levels as the Chua's case.

Secondly the CTS to study was from the attractor of Fig. 7d. Figure 12a shows 0.01 seconds of CG data, 400 points of the series. The variance plot of the wavelet coefficients is shown in Fig. 12b. We can observe a maximum in the plot at level $m = 14$. In Fig. 12c the 14th level is plotted, and we see that this scale corresponds to the energy concentration of the CTS, with a slight downward translation, because of the DC component of this CTS.

The final CTS to consider comes from the attractor of Fig. 7f, and is shown in Fig. 13a. This CTS has a "regular" pattern. The variance plot [Fig. 13b] shows an energy concentration at levels $m = 12$, $m = 14$, and perhaps at $m = 13$. Note that the behavior of this log variance shows a great similarity with the CTS of the Rössler system, with the exception of the decreasing level $m = 13$. Figure 13c shows that the sum of the 12th and 14th wavelet levels has the high energy concentration of the CTS.

The attractors in Figs. 7a, c and e, have a similar behavior to that of the attractors in Figs. 7b, d and f, respectively.

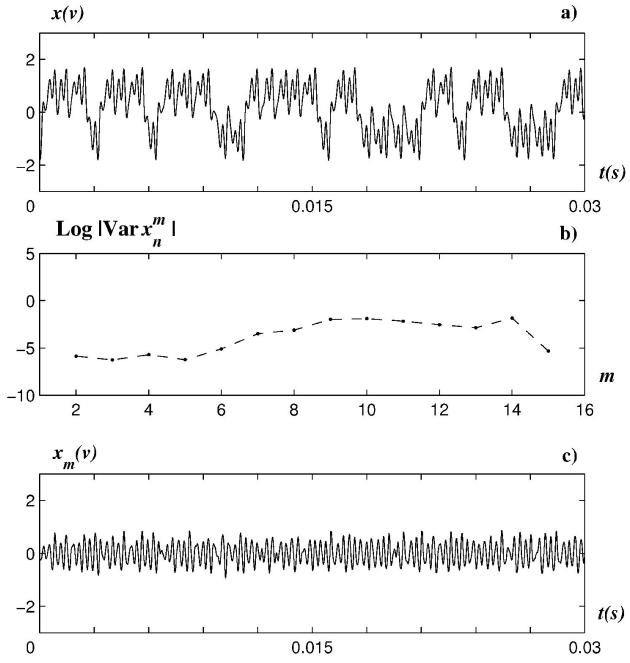


FIGURE 11. a) Experimental time data for CG system of Fig. 7b, b) wavelet coefficient variance, and c) 14th wavelet level.

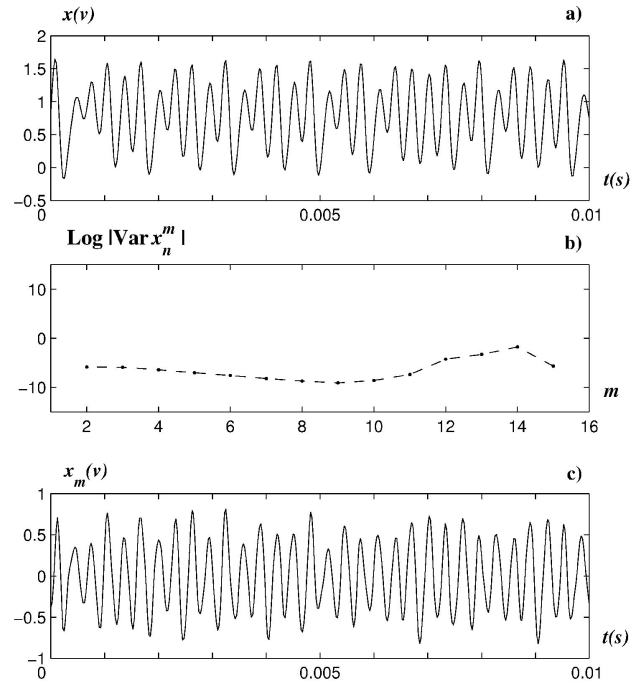


FIGURE 12. a) Experimental time data for CG system of Fig. 7d, b) wavelet coefficient variance, and c) 14th wavelet level.

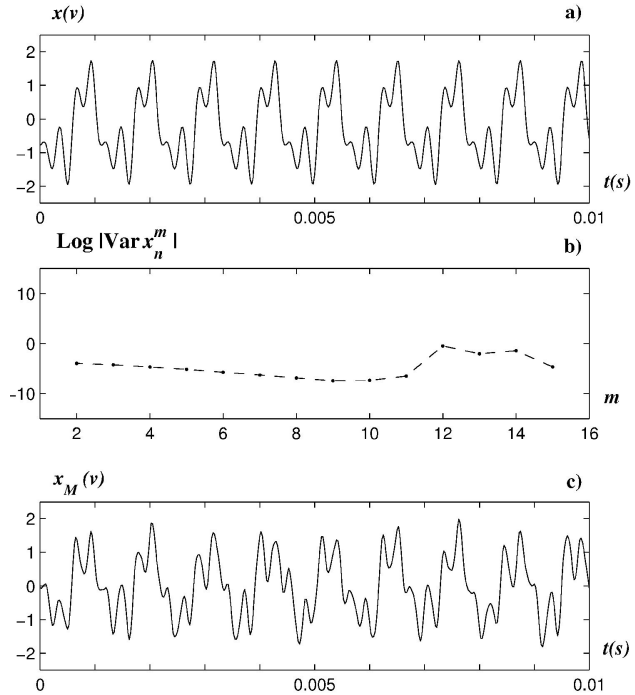


FIGURE 13. a) Time experimental data for CG system of Fig. 7f, b) wavelet coefficient variance, and c) sum of the 12th and 14th wavelet levels.

## 5. Conclusions

We have analyzed some experimental CTS using the discrete wavelet transform, with a simple statistical approach. In order to obtain useful information about chaotic systems, this discrete transform has been applied to time series that come from three experimental chaotic oscillators, the Chua, Rössler and CG systems. For the experimental CTS from Chua's system, we observed that there is no energy concentration at specific wavelet levels of the log variance. In fact, this CTS would seem to have a noise behavior; the gradient of the log variance is close to zero. For this CTS, we see how a wavelet function gives more representative information of the signal than another wavelet function. For the CTS from the attractor of Fig. 7b, corresponding to the CG system, this also does not present any energy concentration. On the other hand, the experimental CTS from the Rössler system presents energy concentration at two wavelet levels of the log variance. In this case, we consider that the sum of these wavelet levels should be considered the carrier frequency of the CTS. A different situation was presented in [3], where this system was numerically analyzed, and it showed an energy concentration at just one level. In addition, the last CTS from the CG system presented an energy concentration in one and two wavelet levels, respectively. We can conclude that the maximum values at the higher wavelet levels, in the log variance plot, provides high energy concentration, and it could correspond to the "carrier" frequency of the CTS.

Despite the fact that we do not go deeply into the pros and cons of using one wavelet over another, we consider, in order to have a more complete analysis, that we should use analyzing wavelets that bear a reasonable resemblance in form to the function or signal.

Finally, there are a variety of methods for analyzing time series, but without a doubt the method based on wavelet analysis is one of the most appealing, and successful, ones. In addition, for the first time to our knowledge, we apply this wavelet analysis to experimental CTS, and we hope that these results will inspire a further use of wavelet analysis for chaotic time series.

## Acknowledgement

JSM received partial financial support from PROMEP under contract 103.5/03/1118, and FAI–UASLP under contract C03-FAI-04-23.24, and ECC received partial financial support from FAI-UASLP under contract C04-FAI-10-30.73.

1. H.D.I. Abarbanel, *Analysis of Observed Chaotic Data* (Springer, New York, 1996).
2. G.W. Wornell and A.V. Oppenheim, *IEEE Trans. Inform. Theory* **38** (1992) 785.
3. W.J. Staszewski and K. Worden, *Int. Journal of Bif. and Chaos* **3** (1999) 455.
4. T.L. Carroll, *Am. J. Phys* **63** (1995) 377.
5. E. Campos-Cantón and J.S. Murguía, submitted to publication (2005).
6. L.O. Chua, L. Kocarev, K. Eckert, and M. Itoh, *Int. J. Bif. and Chaos* **2** (1992) 705.
7. N.F. Rulkov, *Chaos* **6** (1996) 262.
8. J. Urías, *Rev. Mex. Fís.* **45** (1999) 331.
9. E. Ott, T. Sauer, and J.A. Yorke, *Coping with Chaos* (John Wiley & Sons, New York, 1994).
10. I. Daubechies, *Ten lectures on Wavelets* (SIAM, Philadelphia, PA, 1992).
11. S. Mallat, *A Wavelet Tour of Signal Processing*, 2nd. Edition (Academic Press, 1999).
12. S. Qian, *Introduction to Time-Frequency and Wavelet Transforms* (Prentice Hall PTR, 2002).
13. G. Strang and T. Nyugen, *Wavelets and Filter Banks* (Prentice Hall, 1996).